Prediction of Nanoparticle Photoreactivity in Mixtures of Surface Foulants Requires Kinetic (Non-Equilibrium) Adsorption Considerations

Riya A. Mathew[1], Marfua Mowla[1], Sheyda Shakiba[1], Tchemongo B. Berté,[1] and Stacey M. Louie[1*]

[1]*Department of Civil & Environmental Engineering, University of Houston, Houston, TX 77004, USA*

***Corresponding Author:**

Address: 4226 Martin Luther King Blvd, Engineering Building 1, Rm N107, Houston, TX 77204-4003

Phone: (713)743-8646

Email: slouie@uh.edu

Revision Submitted to *Environmental Science & Technology*

Abstract

The adsorption of foulants on photocatalytic nanoparticles can suppress their reactivity in water treatment applications by scavenging reactive species at the photocatalyst surface, screening light, or competing for surface sites. These inhibitory effects are commonly modeled using the Langmuir-Hinshelwood model, assuming adsorbed layer compositions follow Langmuirian (equilibrium) competitive adsorption. However, this assumption has not been evaluated in complex mixtures of foulants. This study evaluates the photoreactivity of titanium dioxide (TiO_2) nanoparticles toward a target compound, phenol, in the presence of two classes of foulants: natural organic matter (NOM), protein (bovine serum albumin, BSA), or mixtures of the two. Langmuir adsorption models predict that BSA should strongly influence the nanoparticle photoreactivity because of its higher adsorption affinity relative to phenol and NOM. However, model evaluation of the experimental phenol decay rates suggested that neither the phenol nor foulant surface coverages are governed by Langmuirian competitive adsorption. Rather, a reactivity model incorporating kinetic predictions of adsorbed layer compositions (favoring NOM adsorption) outperformed Langmuirian models in providing accurate, unbiased predictions of phenol degradation rates. This research emphasizes the importance of using first-principles models that account for adsorption kinetics when assumptions of equilibrium adsorption do not apply.

Keywords: Photoreactivity, nanoparticles, titanium dioxide, Langmuir-Hinshelwood model, natural organic matter, bovine serum albumin

Synopsis: Kinetic (non-equilibrium) adsorption models are required to accurately predict the photocatalytic treatment efficiency of TiO_2 nanoparticles toward pollutants in mixtures of surface foulants (natural organic matter and proteins).

Introduction

Photocatalytic nanomaterials are of broad interest for nano-enabled water treatment,[1] with much recent work focused on developing improved materials or reactors.[2-7] However, their water treatment efficiency can be hindered in matrices containing background salts and organic matter.[8-12] Photocatalysis involves the following steps: adsorption of reactants on the catalyst surface; light-activated generation of charge carriers (electron-hole pairs) that can react directly with pollutants or with water or dissolved oxygen to form reactive oxygen species (ROS); and desorption of reaction products.[13-16] Foulants in natural waters, including humic substances and biomolecules such as proteins, often inhibit reactivity toward target pollutants by competing for surface adsorption sites, screening light, or scavenging ROS or charge carriers.[9,10,17-20] Natural organic matter (NOM) can alternatively enhance reactivity in some cases.[9,21-23] Considering that different waters have varying foulant compositions, models capable of predicting reactivity in complex matrices would be useful to estimate the photocatalytic efficiency of nanomaterials for water treatment, as well as in natural environments where they may cause ecotoxicity.[24-27]

Prior studies on the photocatalytic degradation of pollutants in the presence of NOM were summarized by Uyguner-Demirel et al.[10] for titanium dioxide nanoparticles (TiO_2 NPs), one of the most widely studied photocatalysts; additional discussion of modeling is provided in the Supporting Information (SI) Table S1. Many studies either lack quantitative modeling or fit pollutant degradation to a pseudo-first-order model to compare rate constants with versus without foulants. To predict reaction rates across a range of reactant concentrations, the Langmuir-Hinshelwood (L-H) model is commonly used, which incorporates an adsorption component (surface coverage of each reactant) and reaction component (rate constant for each reactant).[28-32] In the first-principles derivation of this model, the surface coverage of each adsorbate is specified

without assuming any particular adsorption isotherm. However, most studies implicitly assume a Langmuir equilibrium adsorption isotherm. This assumption has already been debated with respect to whether adsorption equilibrium is maintained *during the reaction* – i.e., whether the rate-limiting step is the photocatalytic generation of electron/hole pairs or ROS, rather than contaminant adsorption or product desorption from the photocatalyst surface.[29,33,34] Hence, two studies incorporated reactant mass transfer kinetics into the L-H model.[18,19] However, these studies only modeled degradation in the presence of a single type of foulant.

Here, we highlight two additional assumptions that are often overlooked: the assumption that all reactants are competing for the same active sites on the photocatalyst surface, and the assumption that multiple adsorbates will all exhibit Langmuirian (equilibrium) competition. Macromolecular foulants (e.g., polymers, NOM, and proteins) often do not fully coat the entire catalyst surface, so unoccupied sites may always remain available to small target compounds. Additionally, adsorption equilibrium may not be achieved on the photocatalyst surface, even *prior to* initiating the reactions, if the adsorption of any species is irreversible. Macromolecules exhibit resistance to desorption when multiple functional groups along the molecule attach to the surface or when strong surface complexation occurs, e.g., via calcium bridging.[35] Hence, these molecules can remain adsorbed after disequilibration (e.g., washing into adsorbate-free media) and can also resist displacement by higher affinity species. Our prior study found that the adsorbed layer composition on TiO_2 in mixtures of NOM and a model protein, bovine serum albumin (BSA), was controlled by adsorption kinetics rather than equilibrium predictions, i.e., the more rapidly adsorbing species (NOM) outcompeted the higher affinity species (BSA).[36] Small molecules would likewise diffuse more rapidly to the photocatalyst surface. We hypothesize that in this scenario, Langmuirian assumptions will fail to predict the correct surface coverages of the

adsorbates for the L-H model; rather, kinetic adsorption models will be required. Despite the simplicity of this hypothesis, to our best knowledge, it has not been tested for photocatalytic nanomaterials in complex media containing multiple classes of macromolecular foulants. This research gap could be attributable to the analytical challenges in measuring adsorption from mixed foulant solutions, which is needed to predict adsorbed layer compositions for reactivity models.

The objective of this study is to predict the photoreactivity of TiO_2 NPs toward a target compound, phenol, in mixtures of foulants (Suwannee River NOM and BSA). Phenol has been used as a probe for hydroxyl radical generation from TiO_2 NPs.[37] Here, the TiO_2 NPs in the photoreaction experiments were immobilized onto glass rods to achieve a consistent aggregation state across various foulant exposures in moderately hard water (MHW). Immobilized NPs are also more feasible for application because NP separation steps are not required post-treatment.[2,8] Photocatalytic degradation of phenol was systematically evaluated in systems of increasing complexity (phenol alone, in the presence of individual foulants, or in mixtures of NOM and BSA). Following this approach, the reaction models were incrementally parameterized and ultimately compared to evaluate the suitability of assuming Langmuirian competitive equilibrium in the L-H model, as opposed to kinetically-predicted surface coverages of NOM and BSA.

Theory and Approach

Reaction in the absence of inhibitory species at varying target compound concentrations

The surface-mediated photocatalytic oxidation of a probe or target compound (here, phenol) in the absence of inhibitory foulants (e.g., BSA and/or NOM) can be modeled by Equation 1, as derived in SI Section S2 following theory presented by Loddo et al.[28] for heterogeneous catalysis:

$$\frac{dC_{\text{target}}}{dt} = k'_{\text{target}}\theta_{\text{ox}}\theta_{\text{target}} = k'_{\text{phenol}}\theta_{\text{ox}}\theta_{\text{phenol}} \quad (1)$$

where dC_{target}/dt is the rate of loss of the target compound over time (mg L^{-1} h^{-1}), k'_{target} is a rate constant (mg L^{-1} h^{-1}) for reaction of target compound (phenol) with oxidant, and θ_{ox} and θ_{target} (unitless) are the fractional surface coverages of oxidant ("ox") and target compound, respectively, on the active sites of the photocatalyst. If the phenol adsorption is assumed to follow a Langmuir isotherm and the oxidant concentration is assumed to be a constant, $\theta^{\circ}_{\text{ox}}$ (where the superscript ° denotes the absence of inhibitory species), then Equation 2 follows:

$$\frac{dC_{\text{target}}}{dt} = k'_{\text{target}}\theta^{\circ}_{\text{ox}}\left(\frac{K_{\text{target}}C_{\text{target}}}{1 + K_{\text{target}}C_{\text{target}}}\right) = k'_{\text{phenol}}\theta^{\circ}_{\text{ox}}\left(\frac{K_{\text{phenol}}C_{\text{phenol}}}{1 + K_{\text{phenol}}C_{\text{phenol}}}\right) \quad (2)$$

where K_{target} is the Langmuir isotherm constant (L mg^{-1}) for the target compound.

<u>Reaction in the presence of inhibitory species at a fixed target compound solution concentration</u>

When introducing inhibitory species, *i* (e.g., BSA and/or NOM), the initial phenol concentration was fixed at a single concentration (5 mg L^{-1}) while varying the foulant concentrations. The measured degradation rate and fraction of surface active sites occupied by the target compound are represented by the constants $r^{\circ}_{\text{target}}$ (mg L^{-1} h^{-1}) and $\theta^{\circ}_{\text{target}}$ (unitless), respectively, where the superscript ° here denotes the fixed target solution concentration in the absence of inhibitory species. Following Schwarzenbach et al.,[38] an oxidant mass balance is written, assuming that the oxidant production rate at the catalyst surface is constant, and the steady-state oxidant concentration is depleted by reaction with the inhibitors in addition to background

reactions with species other than the target or inhibitory compounds, e.g. salts in the reaction media. Incorporating the oxidant concentration into Equation 1 yields Equation 3 (derivation in SI Section S2):

$$\frac{dC_{\text{target}}}{dt} = \frac{r^{\circ}_{\text{target}}}{1 + \sum_i (k_i \theta_i)} \left(\frac{\theta_{\text{target}}}{\theta^{\circ}_{\text{target}}} \right) = \frac{r^{\circ}_{\text{phenol}}}{1 + k_{\text{BSA}} \theta_{\text{BSA}} + k_{\text{NOM}} \theta_{\text{NOM}}} \left(\frac{\theta_{\text{target}}}{\theta^{\circ}_{\text{target}}} \right) \quad (3)$$

where θ_{target} and θ_i (unitless) are the fractions of surface active sites occupied by the target and inhibitory species, respectively, in the samples with foulants; and k_i (unitless) is a lumped reaction rate constant defined as $k_i \equiv \frac{A_{\text{ox}/i} k_i'}{B}$, where $A_{\text{ox}/i}$ is a stoichiometric coefficient (mass of oxidant per mass of inhibitory species, *i*), k_i' is a zero-order rate constant (mg L^{-1} h^{-1}) for reaction of *i* with oxidant, and *B* is a constant (mg L^{-1} h^{-1}) representing the rate of oxidant depletion by background reactions.

Equation 3 shows that the decay rate of the target compound can be suppressed by competition for adsorption sites influencing θ_{target}, as well as scavenging as represented by $k_i' \theta_i$ for the surface foulants. Three implementations of this model were evaluated with different assumptions on the active site competition:

(1) *Target compound adsorption is suppressed by the inhibitors, and all species' surface coverages are predicted by Langmuirian competitive adsorption*

If all species (target compound and foulants) compete for active sites, then the Langmuir predictions for surface coverages are given by Equation 4:

$$\theta_m = \frac{q_m}{q_{\max,m}} = \frac{K_m C_m}{1 + \sum_n (K_n C_n)} = \frac{K_m C_m}{1 + K_{\text{phenol}} C_{\text{phenol}} + K_{\text{BSA}} C_{\text{BSA}} + K_{\text{NOM}} C_{\text{NOM}}} \quad (4)$$

where m represents the specific adsorbate of interest (phenol, BSA, or NOM), n represents all competing adsorbates, q_m is the adsorbed mass of m (mg m^{-2}), $q_{\max,m}$ is the maximum adsorbed mass of m (mg m^{-2}), K_m and K_n are the Langmuir isotherm constants (L mg^{-1}), and C_m and C_n are the bulk solution concentrations (mg L^{-1}) of m and n, respectively. Equation 3 then becomes Equation 5:

$$\frac{dC_{\text{target}}}{dt} = \frac{r^{\circ}_{\text{target}}}{1 + \sum_i \left[k_i \left(\frac{K_i C_i}{1 + K_{\text{target}} C_{\text{target}} + \sum_i (K_i C_i)} \right) \right]} \left[\frac{K_{\text{target}} C_{\text{target}} / (1 + K_{\text{target}} C_{\text{target}} + \sum_i (K_i C_i))}{K_{\text{target}} C_{\text{target}} / (1 + K_{\text{target}} C_{\text{target}})} \right] \quad (5)$$

where i includes only the inhibitory species (BSA and NOM).

(2) *Target compound adsorption is not affected by the inhibitors, whereas inhibitors compete for adsorption sites following Langmuirian competitive adsorption*

If the foulants compete with each other following Langmuirian competition but do **not** compete with the target compound for active sites (i.e., they induce negligible displacement of target compound, and vice versa), then θ_{target} with foulants is equivalent to $\theta^{\circ}_{\text{target}}$ without foulants, and the target compound is also excluded from the foulant adsorption predictions, resulting in Equation 6:

$$\frac{dC_{\text{target}}}{dt} = \frac{r^{\circ}_{\text{target}}}{1 + \sum_i \left[k_i \left(\frac{K_i C_i}{1 + \sum_i (K_i C_i)} \right) \right]} \quad (6)$$

(3) *Target compound adsorption is not affected by the inhibitors, whereas inhibitors compete for adsorption sites following a kinetic competitive adsorption model*

This study questions the suitability of the Langmuir competitive adsorption assumption to predict the surface coverages of the foulants and hence the degradation rate for the target compound. In particular, a previous study from our group[36] developed and experimentally validated a kinetic adsorption model for NOM and BSA adsorption to TiO_2 NPs in a MHW background:

$$\ln\left(\frac{N_i}{N_{0,i}}\right) = -4\pi D\left(R_i + R_{\mathrm{TiO_2}}\right)N_{\mathrm{TiO_2}}t \quad (7)$$

$$\theta_i\left(t_{\mathrm{stop},i}\right) = \frac{q_i(t_{\mathrm{stop},i})}{q_{\mathrm{max},i}} = \frac{K_i C_i(t_{\mathrm{stop},i})}{1 + K_i C_i(t_{\mathrm{stop},i})}\left[1 - \sum_j \frac{q_j(t_{\mathrm{stop},i})}{q_{\mathrm{max},j}}\right] \quad (8)$$

Equation 7 is the Smoluchowski collision equation representing the depletion rate of adsorbate from bulk solution upon collision with TiO_2 NPs. N_i and $N_{0,i}$ are the number concentrations of dissolved species, i, at time t and time 0, respectively; N_{TiO2} is the number concentration of TiO_2 NPs; D is the summed diffusion coefficients for i and TiO_2; and R_i and R_{TiO2} are the hydrodynamic radii of i and TiO_2, respectively. Adsorbed masses are computed by dividing the depleted adsorbate concentration by the TiO_2 surface area. Equation 8 is used as a criterion to stop adsorption when each species, i, from the mixture of all adsorbates, j, has met the thermodynamic (Langmuir) predictions with respect to the adsorption sites remaining at $t_{\mathrm{stop},i}$ (but not necessarily with respect to all adsorption sites initially available). When the NPs are simultaneously exposed to NOM and BSA, this model produced better predictions of adsorbed layer compositions than the Langmuir model because NOM had more rapid collision kinetics and adsorption was irreversible, i.e., NOM was not displaced despite the higher affinity of BSA.

Resistance to displacement is also observed in sequential exposure of NOM alone followed by BSA,[36] and vice versa,[39] although adsorption reversibility can depend on the water and surface chemistry, e.g., presence of phosphates.[22,23,40] It is noted that the kinetic model predicts collision rates with TiO_2 to be at least two orders of magnitude higher for phenol at 5 mg L^{-1} than for BSA or NOM at their highest concentrations (100 mg L^{-1}), so the kinetic model would predict that phenol adsorption should not be strongly impacted by the inhibitors. Hence, Equation 3 is simply written as Equation 9:

$$\frac{dC_{\text{target}}}{dt} = \frac{r^{\circ}_{\text{target}}}{1 + \sum_i (k_i \theta_{i,\text{kinetic}})} \quad (9)$$

where $\theta_{i,\text{kinetic}}$ represents the kinetically predicted inhibitor surface coverages.

Light screening and bulk photolysis

The possibility for the NOM and BSA to participate in two other processes influencing the phenol degradation (light screening and bulk photolysis in solution) was also incorporated into the data analysis by including these processes in the mass balance as a screening factor on the oxidant reactions and a second independent phenol decay process for bulk photolysis. Model derivation is provided in SI Section S2.3.

Model fitting approach

A stepwise approach was taken to parameterize and evaluate the reaction models. First, target compound decay rates were measured at varying initial phenol concentrations. The data were fitted to Equation 2 to obtain two fitting parameters: K_{phenol} and $(k'_{\text{phenol}}\theta^{\circ}_{\text{ox}})$. This approach

229 was required to estimate K_{phenol} because batch adsorption experiments showed no measurable
230 phenol adsorption onto the TiO_2 nanoparticles. These experiments also provided the values for
231 r^{o}_{phenol}, measured at 5 mg L^{-1} initial phenol concentration, and θ^{o}_{phenol}, computed using K_{phenol}.

232 Adsorption isotherms were measured separately for NOM and BSA to determine $q_{max,i}$ and
233 K_i. Then, phenol decay rates were measured in the presence of single foulants (BSA or NOM only),
234 and mixtures of the two foulants. When all species (including phenol) are assumed to participate
235 in Langmuir competition for active sites, Equation 5 was first applied to the single foulant data,
236 where each data set (BSA or NOM) has only one fitting constant each, i.e., k_{BSA} or k_{NOM}. Since
237 r^{o}_{phenol}, θ^{o}_{phenol}, and k_i were previously quantified and θ_i can be computed using the Langmuir
238 competitive adsorption model, there are no unknown parameters in the mixed foulant cases –
239 hence, the modeled phenol decay rates are evaluated in a purely predictive manner against the
240 measured rates. When constant phenol coverage is assumed, Equation 6 was fitted to determine k_i
241 for the single foulant data. Equations 6 and 9 for the Langmuir and kinetic adsorption models,
242 respectively, were then computed and compared for the mixed foulants (again with no fitting
243 parameters). Note that for single foulants, the kinetic model gives the same predictions as the
244 Langmuir model since the NOM and BSA are not competing with each other.

245 To correct for screening and bulk photolysis, experimental data were collected to measure
246 screening factors and bulk photolysis rates. All measured decay rates were adjusted to compute
247 only the surface reaction component using SI Equation S15. The same model fitting approaches
248 above were then applied to the adjusted decay rates.

249

Materials and Methods

Chemical Reagents

TiO_2 NPs (Aeroxide P25, Evonik Industries, Essen, Germany), titanium isopropoxide (Acros Organics, Morris Plains, NJ), diethanolamine (99%, Alfa Aesar, Ward Hill, MA), and isopropanol (ACS grade, Electron Microscopy Sciences, Hatfield, PA) were used for sol-gel synthesis to immobilize the TiO_2 NPs. Suwannee River NOM (Cat. No. 2R101N) was procured from the International Humic Substances Society (IHSS, St. Paul, MN), and BSA (reagent grade pure powder) from Sera Care Life Sciences (Milford, MA). Phenol (99.5%, unstabilized, Acros Organics, Morris Plains, NJ) was used as the target compound for degradation. Phosphoric acid (85%, ACS grade, Ricca Chemical, Arlington, TX), Coomassie Brilliant Blue G-250 (MP Biomedicals, Santa Ana, CA) and ethanol (anhydrous USP grade, Decon labs, King of Prussia, PA) were used as Bradford assay reagents. Calcium chloride ($CaCl_2$) (> 97 %, anhydrous, ACS grade, Sigma-Aldrich, St. Louis, MO) and sodium bicarbonate ($NaHCO_3$) (> 99.7 %, ACS grade, Sigma-Aldrich) were used to prepare a simplified MHW matrix.

Preparation of TiO_2 NP Coated Glass Rods

Glass stirring rods (5 mm x 150 mm, Kimble Kimax, DWK Life Sciences, Millville, NJ) were cleaned using Alconox soap solution and rinsed with deionized water, dried, and dip-coated/calcined three times in a P25 NP-enriched sol-gel, following the protocol reported by Carbonaro et al. and Balasubramanian et al.[41,42] and described in the SI. This method was reported to yield a TiO_2 composition of 78% anatase and 22% rutile,[42] which is within the reported 95% confidence interval of (76 ± 3)% anatase and (24 ± 3)% rutile reported for P25.[43] Carbonaro et al. reported that no improvement in photocatalytic efficiency was observed past three dip-coating and

273 calcination cycles, suggesting complete coverage at this point.[42]

274

275 ***Adsorption Isotherms of NOM, BSA, and Phenol on TiO_2 NPs***

276 Adsorption isotherms were quantitatively evaluated on suspensions of TiO_2 NPs that were
277 equilibrated overnight in various concentrations of either pure NOM or pure BSA in a MHW
278 background (0.85 mM $CaCl_2$ and 1.2 mM $NaHCO_3$, pH ≈ 8). The full methods are described in
279 the SI. In brief, adsorption was measured by a solution depletion assay by subtracting the
280 unadsorbed BSA or NOM concentrations from their initial concentrations after separating the NPs
281 by centrifugation. BSA was quantified using the Bradford assay. NOM was quantified by size
282 exclusion chromatography (SEC) using a Superdex 75 10/300 Increase SEC column (Cytiva Life
283 Sciences, Marlborough, MA) on a 1290 Infinity high performance liquid chromatography (HPLC)
284 system (binary pump and autosampler) (Agilent Technologies, Santa Clara, CA), with an Agilent
285 1260 Infinity UV-Vis diode array detector and M9-SEC online TOC detector (Suez Water
286 Technologies, Trevose, PA).[44] Adsorption isotherms were evaluated on triplicate separately-
287 prepared samples.

288 Because the aggregation state of the TiO_2 NPs in suspension varies with foulant
289 concentration and the TiO_2 NPs coated on the glass rods can also show a different aggregation
290 state or surface roughness, foulant adsorption was also evaluated directly on the TiO_2-coated stir
291 rods. The adsorption was qualitatively evaluated by visual color development, either directly for
292 NOM by its inherent yellow color or after staining the adsorbed BSA with Bradford reagent.
293 Methods are described in the SI.

294 Quantification of phenol adsorption was attempted at varying phenol concentrations (1, 2,
295 5, 10 mg L^{-1}) on 10 g L^{-1} TiO_2 in MHW for 2 mL total volume. Samples were allowed to equilibrate

for 3 h on an end-over-end rotator at 25 rpm, then centrifuged at 13000 rpm (11337 *g*) for 15 min to pellet the TiO_2 NPs (MiniSpin Plus, Eppendorf, Enfield, CT). Supernatants were filtered using a 0.22 μm PTFE filter (MicroSolv, Leland, NC) and transferred to HPLC vials to analyze phenol concentrations on an Agilent 1260 Infinity II system comprising a binary pump, refrigerated autosampler (4 °C) with temperature-controlled column compartment (25 °C), Agilent Zorbax Eclipse Plus C_{18} HPLC column (4.6 x 150 mm, 5 μm) with a Phenomenex C_{18} guard column, and UV-Vis detection (methods in SI). The high TiO_2 concentration was used because phenol adsorption was anticipated to be low.[23]

Size and Electrophoretic Light Scattering Measurements

The hydrodynamic sizes of the TiO_2 suspensions used in the adsorption isotherms were measured by dynamic light scattering (DLS) (Zetasizer Nano ZS, Malvern Panalytical, Malvern, UK). Zeta potentials were measured by electrophoretic light scattering on the Zetasizer Nano ZS using a folded capillary zeta cell (DTS1070, Malvern) with automatic voltage selection (150 V), using the Smoluchowski approximation to convert electrophoretic mobility to zeta potential.

Photocatalysis Experiments

Degradation of phenol at (5, 10, 20, and 40) mg L^{-1} was first measured using bare TiO_2-coated rods (without foulants) in MHW. Irradiation was conducted on 10 mL of sample in quartz vials in an annular UV reactor (Rayonet RMR-600, Southern New England Ultraviolet Co., Branford, CT) with a rotating carousel, cooling fan, eight vial positions, and eight fluorescent UV lamps with wavelength centered at 350 nm (Rayonet RMR-3500A) and total irradiance of (5.0 ± 0.2) mW cm^{-2} measured in the UVA/UVB range (UV513AB light meter, GeneralTools, New

York, NY). 1 mL of sample was collected at 1 h intervals from (0 to 5) h. Prior to sample collection, the vial was inverted three times to homogenize. Samples were centrifuged at 13000 rpm for 15 min, and 0.4 mL of supernatant was transferred to an HPLC vial for phenol quantification.

Phenol degradation was also evaluated using TiO_2-coated rods in MHW containing pure NOM or BSA at (0, 10, 25, and 100) mg L^{-1}, or their mixtures at varying concentrations: (10, 25, and 100) mg L^{-1} NOM for fixed BSA concentrations of (10 and 100) mg L^{-1}, and vice-versa. To allow foulant adsorption, the TiO_2 rods were initially placed in dark (foil-wrapped) quartz vials containing NOM, BSA, or the mixtures overnight at room temperature. Then, phenol was added (final concentration of 5 mg L^{-1}). Photoreaction experiments were performed as described above in triplicates. Dark controls were run in foil-wrapped vials for the bare TiO_2 and TiO_2 coated with NOM and BSA at the highest concentrations (100 mg L^{-1} individually or mixed).

Phenol concentrations were analyzed as noted for the adsorption experiments (methods in SI). NOM and BSA degradation was evaluated by SEC analysis of the samples collected at (0 and 5) h, and BSA concentrations were measured by the Bradford assay, as noted for the adsorption isotherms and described in the SI.

Inner Filter Effect and Bulk Photolysis

To quantify the inner filter effect, UV-Vis absorbances were measured from (200 to 800) nm for all NOM and BSA concentrations (separate and mixtures) in MHW without TiO_2 or phenol. The absorbances were applied to the manufacturer's reported UV lamp spectrum (Rayonet RMR-3500A, wavelength range of (300 to 400) nm) to compute the attenuated spectrum reaching the surface of the TiO_2-coated stir rods, as detailed in the SI Section S2.3. The inner filter effect was computed as the ratio of attenuated to unattenuated light intensity integrated across all lamp

wavelengths. To evaluate phenol degradation by bulk photolysis, photoreaction experiments were conducted in the Rayonet photoreactor for 5 mg L^{-1} of phenol in all foulant solutions, using uncoated glass rods in place of TiO_2-coated rods to maintain the same reactor geometry. Experiments were triplicated.

Results and Discussion

Phenol Adsorption and Photoreactivity of Bare TiO_2 in Varying Phenol Concentrations

Phenol adsorption was too low to be reliably measured (i.e., < 10% depletion) even at high TiO_2 concentrations (10 g L^{-1}), consistent with our previous study where phenol adsorption was low whereas its degradation byproducts (catechol and hydroquinone) showed measurable adsorption.[23] Because phenol is a small molecule and its maximum surface coverage is low, it was hypothesized that phenol adsorption will be unaffected by the presence of the surface foulants. Photoreactivity experiments with phenol only, followed by phenol with foulants, were conducted to evaluate this hypothesis.

The photoreactivity of the TiO_2 toward phenol alone was measured over 5 h (SI Figure S1). The photoreactivity model (Equation 2) is based on the initial sample conditions, so the initial phenol degradation rates (computed as the loss from 0 h to 1 h of irradiation) were used to fit the model (Figure 1). The fitted parameters were 4.9 mg L^{-1} h^{-1} for $k'_{\mathrm{phenol}}\theta^{\circ}_{\mathrm{ox}}$ and 0.08 L mg^{-1} for K_{phenol}, indicative of a low affinity isotherm for phenol adsorption onto the TiO_2-coated rods.

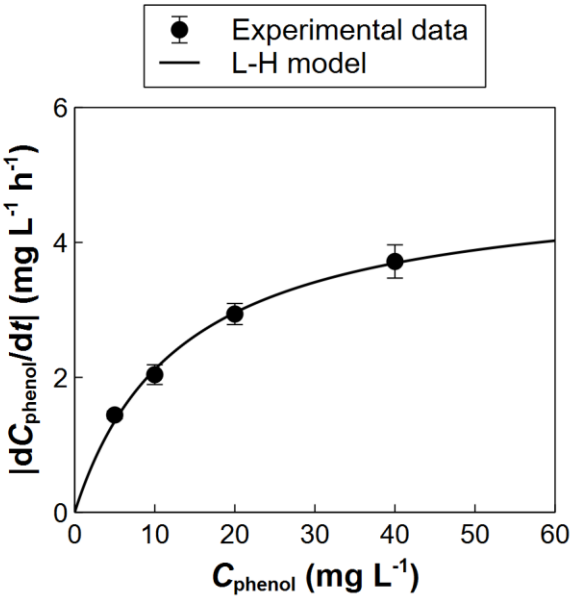

Figure 1. Measured phenol degradation rates for varying concentrations of phenol in MHW, and the best-fit Langmuir-Hinshelwood (L-H) model using Equation 2. Error bars indicate standard deviations across triplicate experiments.

Foulant Adsorption and Photoreactivity of TiO_2 in Individual Foulants

The adsorption of pure BSA or pure NOM on TiO_2 was evaluated by batch adsorption at pH 7.8 to 8, with BSA quantified using the Bradford assay and NOM using SEC-TOC analysis (Figure S2). The adsorbed masses of each foulant were fitted using a Langmuir isotherm (Figure 2a), yielding best-fit parameters for BSA and NOM of (2.1 or 0.6) mg m^{-2}, respectively, for the saturation adsorbed mass, q_{max}, and (0.6 and 0.04) L mg^{-1} for the Langmuir adsorption constant, K. The K values indicate a higher adsorption affinity of BSA than NOM, i.e. the surface is saturated at lower BSA concentrations. The q_{max} values are lower than those in our prior work in MHW at pH 7 (instead of pH 8 here), i.e., 2.6 mg m^{-2} for BSA and 0.9 mg m^{-2} for NOM.[36] The isoelectric point of TiO_2 is ≈ 7,[45] so higher electrostatic repulsion exists between the negatively-charged

adsorbates and negatively-charged TiO_2 surface at pH 8, consistent with lower adsorbed masses. These results suggest that at pH 8, the TiO_2 surface is not completely covered even at saturation concentrations of BSA or NOM, i.e., physical surface area remains where phenol can adsorb.

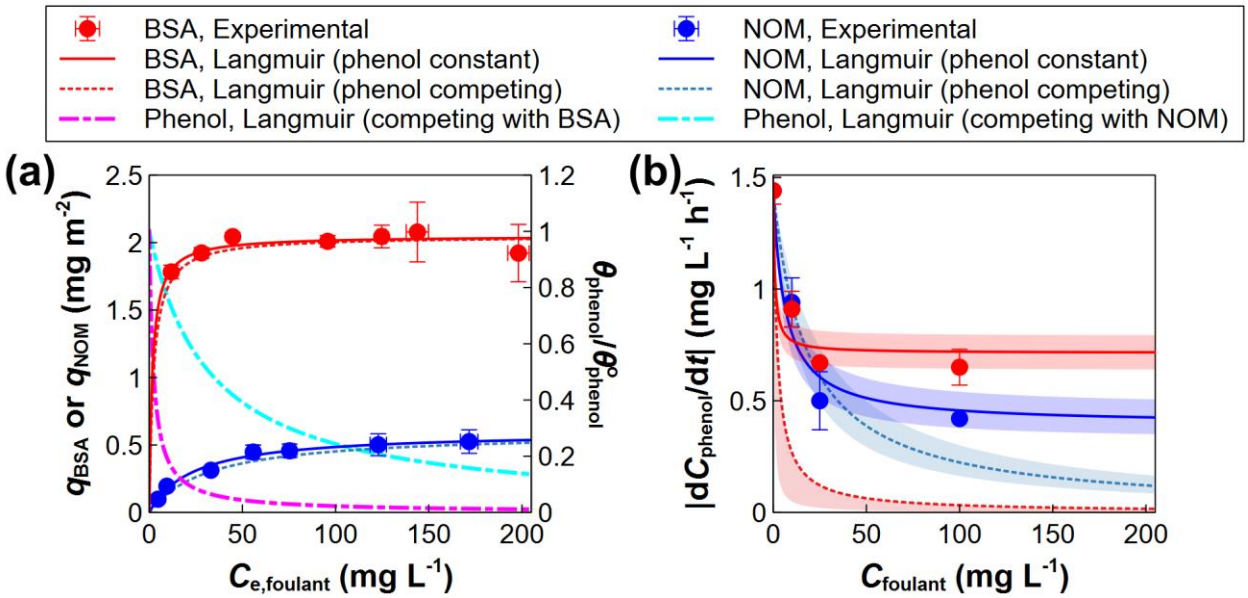

Figure 2. Adsorption isotherms of BSA onto 0.5 g L^{-1} TiO_2 NPs and NOM onto 1 g L^{-1} TiO_2 NPs (a), and the measured and predicted phenol degradation rates using TiO_2-coated glass rods in the presence of separate BSA or NOM solutions (b) in MHW background (0.85 mM $CaCl_2$ and 1.2 mM $NaHCO_3$, pH ≈ 8). Raw data used to determine phenol degradation rates are provided in Figure S5. Solid lines represent the best-fit Langmuir adsorption isotherms (a) and reaction models (b) using Equations 4 (Langmuir, phenol competing) or 5 (Langmuir, phenol constant) for individual foulants. Error bars on experimental data indicate standard deviations across triplicate experiments. Shaded regions were computed using the lower and upper bounds of the 95% confidence intervals on the fitted BSA and NOM rate constants.

The TiO_2 NPs showed a *z*-average diameter of (151 ± 4) nm for stable suspensions in 1 mM NaCl (n = 8 samples). However, the surface potential was screened in MHW, especially by the divalent Ca^{2+} ions (Figure S3). Hence, large agglomerates (> 1 μm) were present despite the more negative zeta potentials and improved colloidal stability conferred by NOM and BSA at high concentrations (Figure S3). For the photoreaction experiments, the TiO_2 NPs were immobilized onto glass rods to avoid variations in agglomeration state, which could influence the reactivity. The P25-enriched sol-gel synthesis was reported to produce similar compositions to the pure P25 NPs used for the adsorption isotherms,[42] but the suspended NP agglomeration and differences in surface roughness or structure for the rod coatings could introduce experimental error in the measured adsorbed masses. Hence, we colorimetrically evaluated the adsorption of both species onto the TiO_2-coated rods (SI Figure S4). The results qualitatively affirm the relative difference in adsorption affinity (the most important parameter in the photoreactivity models): BSA showed strong color after staining at both low (10 mg L^{-1}) and high (100 mg L^{-1}) foulant concentrations, whereas NOM showed greater changes in color from (10 to 25 to 100) mg L^{-1} (Figure S4). For the modeling equations, the surface area of the TiO_2-coated rods (≈ 0.18 cm^2 per mL of solution, not accounting for surface roughness) is orders of magnitude lower than that in the adsorption experiments using TiO_2 suspensions (270 cm^2/mL for BSA and 540 cm^2/mL for NOM). Therefore, no significant depletion of the dissolved concentration of foulant occurs in the photoreaction experiments. Hence, C_i in the reactivity models was taken to be the initially added concentration of BSA or NOM to compute adsorbed masses for the immobilized TiO_2 NPs.

The photoreactivity of the TiO_2 toward phenol (initial concentration of 5 mg L^{-1}) in the presence of individual foulants was assessed by the initial phenol degradation rates (Figure 2(b)). Pseudo-first-order rate constants were also fitted over the entire 5 h experiments (Figures S5 and

S6 for individual foulants and mixtures, respectively) and generally correlated with the initial rate (Figure S7), so the rates determined by either approach would yield similar modeling results. Dark controls indicated negligible loss of phenol without irradiation (data not shown). Bare TiO_2 showed the highest phenol degradation rate of (1.44 ± 0.06) mg L^{-1} h^{-1}, or (8.2 ± 0.3) × 10^{-4} mol phenol per mol photons incident on the TiO_2, computed as described in SI Section S2.3, whereas increasing concentrations of either foulant suppressed the reactivity (Figure S5 and Figure 2(b)), which could be attributable to oxidant scavenging or light screening. All data were first modeled considering oxidant scavenging only; light screening and bulk photolysis are incorporated later.

Individual foulant results were evaluated assuming phenol competes for the same active sites as BSA and NOM (Equation 5) or constant phenol coverage (Equation 6). If all species compete for adsorption sites, both foulants are predicted to strongly suppress phenol adsorption (Figure 2a) because of the higher mass concentrations of both foulants relative to phenol, as well as the higher adsorption affinity of BSA. In Equation 5, the phenol surface coverage can be interpreted as setting a maximum reactivity relative to the bare TiO_2, with additional suppression by oxidant scavenging. Fitted rate constants are presented as the best-fit value followed by the 95% confidence interval range on the fitted parameter in parentheses (determined using SI Equation S16 following Bates and Watts.[46] The fitted rate constants were k_{BSA} = 0 (0, 5.5) and k_{NOM} = 0.8 (0.2, 1.5). The bounds of each confidence interval were used to plot confidence bands on the model fits, with the upper and lower scavenging rates corresponding to lower and higher reactivity, respectively (Figure 2b). For NOM, the experimental data fall outside the 95% confidence band of the model prediction at the highest NOM concentration, where increasing phenol displacement is predicted. The normalized root mean square error (NRMSE) and normalized bias for the best-fit model to the NOM data were 21% and –5%, respectively. For

438 BSA, the experimental data at all concentrations fall outside the 95% confidence band, and the
439 best-fit rate constant is 0 because of the extensive phenol displacement predicted. The NRMSE
440 and normalized bias for the BSA data were 81% and –81%, respectively, with the negative value
441 representing underprediction of phenol decay rates.

442 On the other hand, assuming constant phenol coverage (Equation 6) yields a good fit to the
443 data (Figure 2b), with the 95% confidence bands overlapping error bars on the experimental data
444 for BSA and NOM at all concentrations. The NRMSE and bias were 17% and +0.3% for NOM,
445 and 13% and –0.03% for BSA. These results support the assumption that the foulants only
446 scavenge oxidant proportional to the foulant surface coverage, with negligible phenol
447 displacement. Indeed, the general trend in the suppression of the photoreactivity shows an inverse
448 curve shape to the BSA and NOM adsorption isotherms, i.e., the reaction rate plateaus at higher
449 NOM concentrations rather than continually decreasing, and the BSA suppression of phenol decay
450 is not overpredicted. The fitted rate constants were k_{BSA} = 1.0 (0.8, 1.3) and k_{NOM} = 2.7 (2.1, 3.5),
451 indicating a higher oxidant scavenging rate per adsorbed mass of NOM. Hence, at the higher
452 solution concentrations (25 mg L^{-1} and 100 mg L^{-1}), NOM showed greater inhibition than BSA
453 despite its lower adsorbed mass.

454

455 ***Foulant Adsorption and Photoreactivity of TiO_2 in Foulant Mixtures***

456 The adsorbed layer compositions in the foulant mixtures were predicted using Langmuir
457 or kinetic competitive adsorption models. Cases were systematically evaluated by holding one of
458 the foulants (BSA or NOM) fixed at either a high concentration of 100 mg L^{-1} (Figure 3) or a low
459 concentration of 10 mg L^{-1} (Figure 4), while varying the concentration of the competing foulant
460 from (0 to 100) mg L^{-1}. For these systems, the kinetic model was validated to produce significantly

461 improved predictions of adsorbed layer compositions over the Langmuir model in our previous
462 study.[36] The Langmuir model predicts higher BSA adsorption in all mixtures because of its higher
463 affinity. However, in our prior study,[36] the kinetic model yielded lower model error than the
464 Langmuir model, i.e., lower deviation from experimental observations because the NOM diffuses
465 and hence attaches more rapidly onto the TiO_2 surface, and the NOM adsorption is not reversible
466 under the conditions studied, i.e., BSA does not displace adsorbed NOM.
467

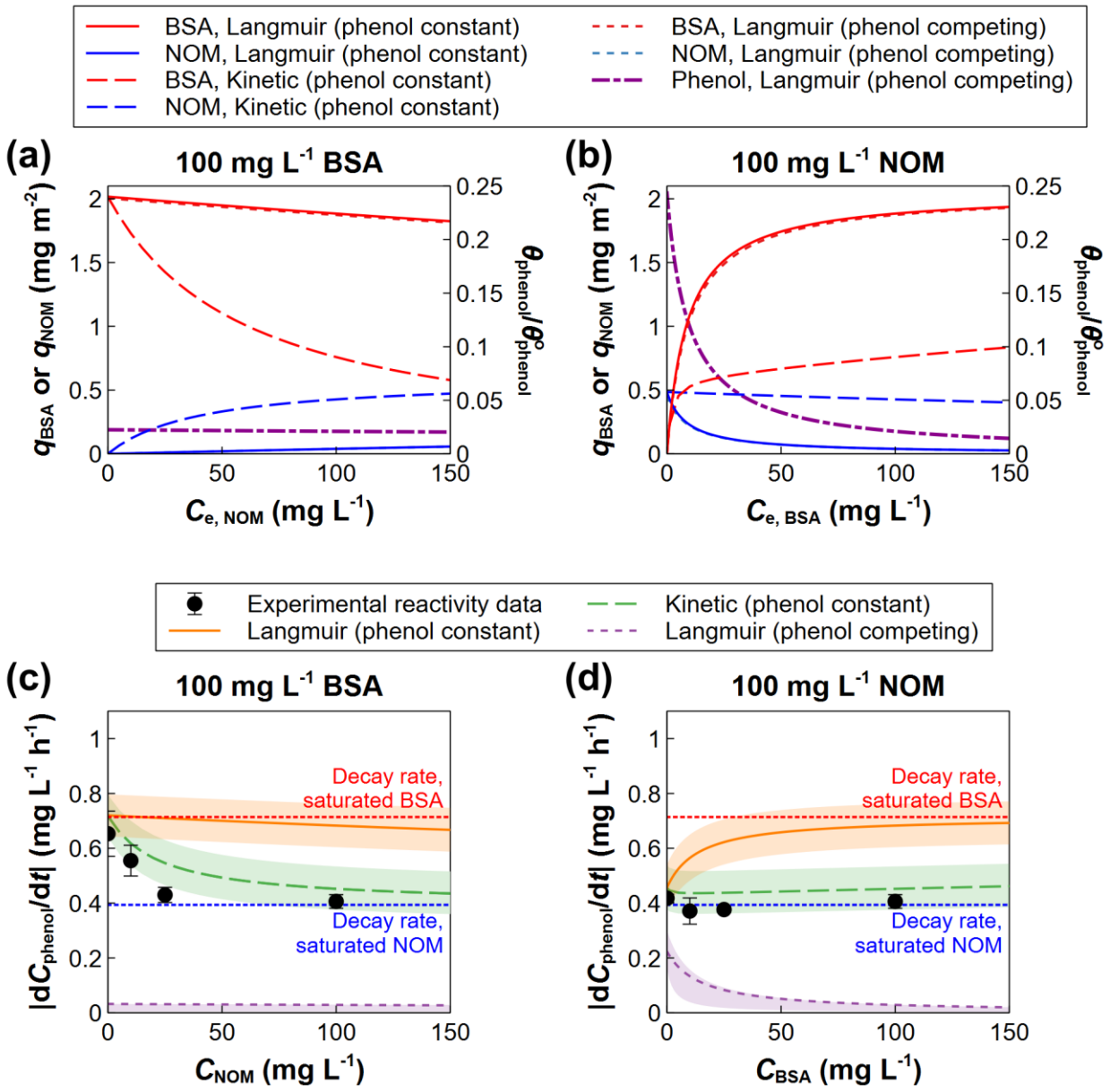

Figure 3. Predicted adsorbed layer compositions (a, b) and measured and predicted phenol degradation rates (c, d) in mixtures of 100 mg L^{-1} of BSA (a) or NOM (b) with varying concentrations of competing adsorbate, comparing Equations 5 (Langmuir, phenol competing), 6 (Langmuir, phenol constant), and 9 (Kinetic, phenol constant). Error bars indicate standard deviations across triplicate experiments. Shaded regions were computed using the lower and upper bounds of the 95% confidence intervals on the fitted BSA and NOM rate constants.

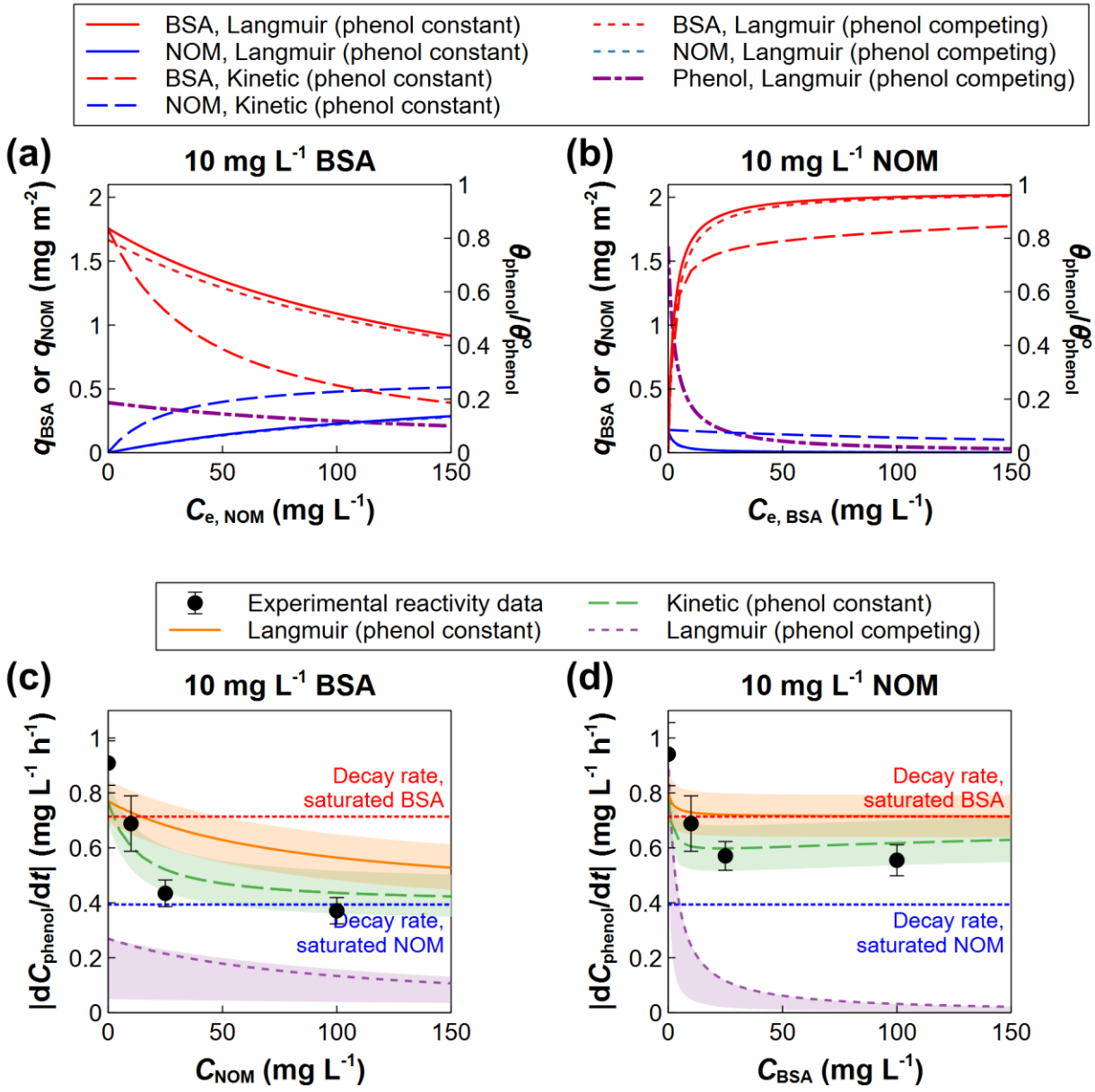

Figure 4. Predicted adsorbed layer compositions (a, b) and measured and predicted phenol degradation rates (c, d) in mixtures of 10 mg L^{-1} of BSA (a) or NOM (b) with varying concentrations of competing adsorbate, comparing Equations 5 (Langmuir, phenol competing), 6 (Langmuir, phenol constant), and 9 (Kinetic, phenol constant). Error bars indicate standard deviations across triplicate experiments. Shaded regions were computed using the lower and upper bounds of the 95% confidence intervals on the fitted BSA and NOM rate constants.

The Langmuir model allowing phenol displacement (Equation 5) predicts extensive suppression of phenol sorption in the mixtures (Figures 3(a,b) and 4(a,b)), which all contain high-affinity BSA. Comparing NOM and BSA surface coverage predictions from the Langmuir and kinetic adsorption models, differences are most apparent at high foulant concentrations where the TiO_2 surface is nearly saturated. For example, when considering a high fixed BSA concentration (100 mg L^{-1}) (Figure 3(a)), the kinetic adsorption model predicts that added NOM will outcompete BSA, whereas the Langmuir model predicts only a small change in the BSA adsorbed mass (< 20% relative to BSA alone) as the NOM concentration increases to 100 mg L^{-1}. For a fixed NOM concentration (100 mg L^{-1}) (Figure 3(b)), the kinetic model predicts a layer comprised primarily of NOM even in BSA concentrations up to 100 mg L^{-1}, whereas the Langmuir model predicts that BSA should dominate the layer even at low BSA concentrations, e.g. ≈ 10 mg L^{-1}. At lower foulant concentrations where the surface is not fully saturated, differences between the two model predictions are still apparent but less substantial because there is lesser competition for surface sites, so BSA has opportunities to adsorb after NOM has reached the TiO_2 surface (Figure 4(a,b)).

The photoreactivity of the immobilized TiO_2 in the foulant mixtures is shown in Figures 3(c,d) and 4(c,d) and compared to model predictions using Equations 5, 6, and 9. The model assuming phenol displacement (Equation 5) could not represent the experimental results for even the single foulant experiments (Figure 2) and likewise fails to predict the mixed foulant results, with high NRMSE (80%) and severe underprediction bias (–77%) from the apparent overprediction of phenol displacement by BSA. Equations 6 and 9 comparing Langmuir versus kinetic adsorption models to estimate foulant layer compositions (with constant phenol coverage) are herewith compared. Limiting cases for a pure foulant layer saturated in BSA or NOM are

505 shown in red and blue, respectively. As shown in Figure 2(b), a saturated BSA layer shows lower
506 oxidant scavenging than a saturated NOM layer. Therefore, the Langmuir adsorption model
507 (favoring the less reactive BSA) consistently predicts lower scavenging, i.e., higher reactivity
508 towards phenol, than the kinetic adsorption model (favoring NOM). In high foulant concentrations
509 (Figure 3), the kinetic model better represents the overall trend in the experimental data, with
510 reactivity approaching that for the saturated NOM layer as the NOM concentration increases in
511 the presence of 100 mg L^{-1} BSA, or remaining near the saturated NOM layer in 100 mg L^{-1} even
512 as the BSA concentration increases to 100 mg L^{-1}. In contrast, the Langmuir model predicts NOM
513 has little impact in 100 mg L^{-1} BSA, and that the less reactive BSA displaces NOM at 100 mg L^{-1},
514 resulting in higher phenol degradation rates (lower scavenging). Notably, the experimental data in
515 all mixtures containing 100 mg L^{-1} of one species fall outside the 95% confidence bands for the
516 Langmuir model. In contrast, all observed data fall within the 95% confidence bands for the kinetic
517 model predictions except 25 mg L^{-1} NOM in 100 mg L^{-1} BSA. The higher observed suppression
518 of reactivity in this mixture could be attributable to NOM complexation with BSA (discussed in
519 the foulant degradation measurements below), which would bring additional NOM to the TiO_2
520 surface via attachment to BSA. When both foulant concentrations are low (e.g., both 10 mg L^{-1})
521 and the surface is undersaturated, there is lesser distinction between the two models (Figure 4).
522 However, as the competing adsorbate concentration increases to 25 mg L^{-1} and 100 mg L^{-1}, only
523 the kinetic adsorption model predicts the observed results within the 95% confidence bands. The
524 overall NRMSE and normalized bias across all mixture samples was 45% and +42%, respectively,
525 for the Langmuir model, in contrast to 15% and +10%, respectively, for the kinetic model.
526

Screening and Bulk Photolysis

In addition to oxidant scavenging, foulants in the bulk solution can influence the phenol degradation rate by the inner filter or screening effect (attenuation of light reaching the TiO_2 surface) and bulk photolysis (reaction of phenol with photosensitized foulants). BSA showed negligible screening in the wavelengths of interest and no significant influence on the bulk photolysis of phenol (Figure S8 and Table S2). On the other hand, NOM produced a strong screening effect: (10, 25, and 100) mg L^{-1} NOM attenuates 5%, 12%, and 40% of the light, respectively. This screening would contribute to lower phenol degradation rates. However, NOM also induced higher rates of bulk photolysis. The reactivity model was rearranged to compute only the surface reaction contribution after adjusting the measured phenol degradation rates for screening and bulk photolysis (Equation S15). After refitting the individual foulant results with these corrections, NOM still shows higher oxidant scavenging than BSA, albeit with a lesser degree of difference (Figure S9). The overall conclusions are the same as in Figures 3 and 4, with Equation 5 (phenol competing) showing the poorest predictions, whereas Equation 9 (kinetic foulant competition, phenol constant) yields more accurate predictions than Equation 6 (Langmuir foulant competition, phenol constant), with only the 25 mg L^{-1} NOM in 100 mg L^{-1} BSA case falling outside the 95% confidence intervals for the kinetic model prediction.

Foulant Degradation

Degradation of the NOM and BSA was evaluated by SEC after 5 h of photoreaction (Figures S10, S11, and S12). Quantitative uncertainties are discussed in SI Section S12. Both BSA and NOM degradation were observed, showing reductions in their original peaks with formation of low molecular weight peaks (degradation products) eluting at later times in the SEC analysis.

In general, the BSA loss and NOM degradation profile were not strongly affected by the presence of each other. This outcome appears counterintuitive to the expectation that increasing competition for oxidants should suppress the degradation of all species, but may suggest that reaction with oxidant is not the rate-limiting step for BSA or NOM degradation. Macromolecules could show kinetic limitations to adsorb or desorb from the TiO_2 surface: Equation 7 computes collision rates with TiO_2 to be at least two orders of magnitude higher for phenol at 5 mg L^{-1} than BSA or NOM at their highest concentrations (100 mg L^{-1}). Interestingly, a higher collision rate is also predicted for BSA monomer than dimer, and greater loss of monomer than dimer was indeed observed by SEC despite their identical chemical makeup. These results further emphasize the importance of kinetics. Predicting BSA and NOM degradation rates may require advanced models that include both adsorption irreversibility and mass transfer limitations during the reaction.

Model Accuracy and Implications

Model errors are summarized in Table 1 and Figure 5, excluding screening and bulk photolysis. In all cases, assuming Langmuir competition between all species including phenol (Equation 5) yields the poorest prediction accuracy, with samples containing BSA showing particularly high NRMSE (≈ 80%) and heavy bias toward underpredicting phenol degradation rates (normalized bias ≈ –80%) because of the assumed displacement of phenol by the foulants. For the foulant mixtures, assuming Langmuir competition between only the foulants (Equation 6) also yields poorer prediction accuracy and higher bias (NRMSE = 45%; normalized bias = +42%) than the kinetic adsorption model (Equation 9) (NRMSE = 15%; normalized bias = +10%) because the Langmuir model overestimates the contribution of BSA to the adsorbed layer and hence

underestimates the degree of oxidant scavenging. Similar conclusions were drawn after correcting for screening and bulk photolysis (SI Table S3 and SI Figure S14).

Table 1. Summary of model errors, excluding screening and bulk photolysis corrections

Sample Set	Model	RMSE ($mg\ L^{-1}\ h^{-1}$)	NRMSE	Bias ($mg\ L^{-1}\ h^{-1}$)	Normalized Bias
Phenol only	Langmuir (Equation 2, Figure 1)	0.06	2%	-0.01	-0.2%
NOM only	Langmuir – Phenol competing (Equation 5, Figure 5a)	0.13	21%	-0.03	-5%
	Langmuir – Phenol constant (Equation 6, Figure 5b)	0.10	17%	0.00	0.3%
BSA only	Langmuir – Phenol competing (Equation 5, Figure 5a)	0.60	81%	-0.60	-81%
	Langmuir – Phenol constant (Equation 6, Figure 5b)	0.10	13%	0.00	-0.03%
Mixtures	Langmuir – Phenol competing (Equation 5, Figure 5a)	0.38	80%	-0.37	-77%
	Langmuir – Phenol constant (Equation 6, Figure 5b)	0.21	45%	0.20	42%
	Kinetic – Phenol constant (Equation 6, Figure 5c)	0.07	15%	0.05	10%

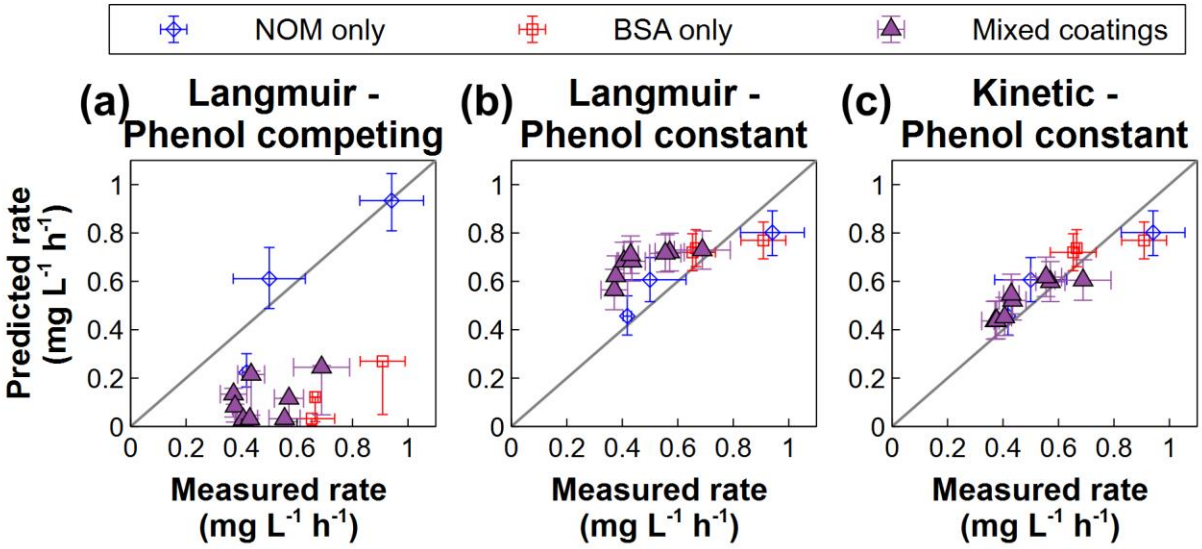

578

579 **Figure 5.** Summary of model predictions using Langmuir (a) or kinetic (b) competitive adsorption
580 models to estimate surface coverages in the surface reactivity model (without accounting for
581 screening or bulk photolysis). Error bars on measured rates represent standard deviations of
582 triplicate measurements, and those on predicted rates were computed from the 95% confidence
583 intervals on the fitted k_{BSA} and k_{NOM} parameters.

584

585 Fundamentally, these results demonstrate the importance of carefully considering
586 assumptions related to competition of all species in the system (target compound and foulants)
587 when implementing competitive reaction models for photoreactive nanomaterials. Often,
588 Langmuirian (equilibrium) competitive adsorption is assumed without confirmatory
589 measurements of layer composition. However, kinetic adsorption models are required to accurately
590 predict surface reactivity when adsorption is irreversible under the time scales considered.
591 Assumptions regarding whether the target and foulant species compete for the same or different
592 adsorption sites, as opposed to only competing for oxidant species, must also be considered.

593 The modeling analysis in this study provided evidence that Langmuir competitive
594 adsorption is not representative of the interactions between any two or three species (phenol as the
595 target compound and NOM or BSA as foulants) to predict the photocatalytic degradation rates of
596 phenol by immobilized TiO_2 NPs in MHW. Comparing the two models assuming constant phenol
597 surface coverage, the Langmuirian predictions deviated from the kinetic predictions by 16% to
598 51%, with higher error when higher concentrations of the foulants (especially NOM) are present.
599 In a photocatalytic water treatment system, other factors such as the reactor geometry and
600 hydrodynamics will be critical to optimize.[32] However, after controlling for these parameters, the
601 observed differences of up to 50% in the reactivity predictions can further translate to
602 corresponding improvements in determining material use efficiency when designing treatment or
603 remediation processes. More broadly, the degree of deviation between the prediction models will
604 also depend on the relative concentrations and scavenging rates of the various foulant constituents.
605 The kinetic adsorption model can hence be useful for photocatalytic water treatment
606 processes that require accurate predictions of reactivity.[32] Kinetic adsorption models can also be
607 pivotal to elucidate the rates and mechanisms of adsorption, and thereby optimize the efficiency,
608 of a variety of other water treatment processes where irreversible adsorption could occur, including
609 heterogeneous catalytic ozonation,[47] adsorption,[48] membrane-based treatment,[43] and wastewater
610 treatment wetlands.[49] These models can also be applied to prioritize the most important foulant
611 species to target for removal in pretreatment operations, prior to applying advanced photocatalytic
612 treatment, or even to inform the design of photocatalyst coatings that prevent NOM fouling without
613 blocking target compound adsorption or scavenging oxidant species. Finally, this knowledge could
614 be useful to understand surface reaction processes in natural aquatic systems and model spatial or
615 temporal variability in surface photocatalysis rates based on water chemistry. Future studies should

further develop advanced reaction models that incorporate both adsorption irreversibility and mass transfer limitations during the reaction process, as well as evaluate the generalizability of the findings for phenol to other target compounds probing a variety of reaction pathways, such as direct hole or electron transfer.

Acknowledgements

This material is based upon work supported by the National Science Foundation Grants No. 1705511 and 2125480, U.S. Department of Energy Grant No. DE-SC0023295, FMC New Investigator Award, Texas Hazardous Waste Research Center Grant No. 110UHH0080H, and Texas Ecolab (Braun & Gresham). We gratefully acknowledge Gokul S. Nair, Anthony S. Chen, and Abdul M. Sohail for preliminary work on immobilizing TiO_2 NPs, Charisma Lattao for general laboratory assistance, and three anonymous reviewers for comments leading to substantial improvements in this research.

Author Information

Equal Contribution: R.A. Mathew, S. M. Louie.

Author Contributions: R.A. Mathew: Investigation, Formal Analysis, Data Curation, Visualization, Writing – Original Draft; M. Mowla: Investigation, Visualization, Writing – Original Draft; S. Shakiba: Formal Analysis; T.B. Berté: Methodology; S.M. Louie: Conceptualization, Data Curation, Visualization, Writing – Original Draft, Writing – Review and Editing, Funding Acquisition, Project Administration, Supervision.

Supporting Information: Literature review; detailed theory and methods; experimental data; modeling of screening and bulk photolysis; foulant degradation.

References

1. Alvarez, P. J. J.; Chan, C. K.; Elimelech, M.; Halas, N. J.; Villagrán, D., Emerging opportunities for nanotechnology to enhance water security. *Nat. Nanotechnol.* **2018,** *13*, (8), 634-641.

2. Loeb, S. K.; Alvarez, P. J. J.; Brame, J. A.; Cates, E. L.; Choi, W.; Crittenden, J.; Dionysiou, D. D.; Li, Q.; Li-Puma, G.; Quan, X.; Sedlak, D. L.; David Waite, T.; Westerhoff, P.; Kim, J.-H., The Technology Horizon for Photocatalytic Water Treatment: Sunrise or Sunset? *Environ. Sci. Technol.* **2019,** *53*, (6), 2937-2947.

3. Suh, M.-J.; Weon, S.; Li, R.; Wang, P.; Kim, J.-H., Enhanced Pollutant Adsorption and Regeneration of Layered Double Hydroxide-Based Photoregenerable Adsorbent. *Environ. Sci. Technol.* **2020,** *54*, (14), 9106-9115.

4. Zhou, X.; Zhao, Y.-Y.; Kim, S.-R.; Elimelech, M.; Hu, S.; Kim, J.-H., Controlled TiO_2 Growth on Reverse Osmosis and Nanofiltration Membranes by Atomic Layer Deposition: Mechanisms and Potential Applications. *Environ. Sci. Technol.* **2018,** *52*, (24), 14311-14320.

5. Zhang, D.; Lee, C.; Javed, H.; Yu, P.; Kim, J.-H.; Alvarez, P. J. J., Easily Recoverable, Micrometer-Sized TiO_2 Hierarchical Spheres Decorated with Cyclodextrin for Enhanced Photocatalytic Degradation of Organic Micropollutants. *Environ. Sci. Technol.* **2018,** *52*, (21), 12402-12411.

6. Lee, C.-G.; Javed, H.; Zhang, D.; Kim, J.-H.; Westerhoff, P.; Li, Q.; Alvarez, P. J. J., Porous Electrospun Fibers Embedding TiO_2 for Adsorption and Photocatalytic Degradation of Water Pollutants. *Environ. Sci. Technol.* **2018,** *52*, (7), 4285-4293.

7. Pelaez, M.; Nolan, N. T.; Pillai, S. C.; Seery, M. K.; Falaras, P.; Kontos, A. G.; Dunlop, P. S. M.; Hamilton, J. W. J.; Byrne, J. A.; O'Shea, K.; Entezari, M. H.; Dionysiou, D. D., A review on the visible light active titanium dioxide photocatalysts for environmental applications. *Appl. Catal., B* **2012,** *125*, 331-349.

8. Westerhoff, P., Reaction: Avoid fairy dust when engineering water-purification technologies. *Chem* **2023,** *9*, (6), 1342-1343.

9. Yang, X.; Rosario-Ortiz, F. L.; Lei, Y.; Pan, Y.; Lei, X.; Westerhoff, P., Multiple Roles of Dissolved Organic Matter in Advanced Oxidation Processes. *Environ. Sci. Technol.* **2022,** *56*, (16), 11111-11131.

10. Uyguner-Demirel, C. S.; Birben, N. C.; Bekbolet, M., Elucidation of background organic matter matrix effect on photocatalytic treatment of contaminants using TiO_2: A review. *Catal. Today* **2017,** *284*, 202-214.

11. Farner Budarz, J.; Turolla, A.; Piasecki, A. F.; Bottero, J.-Y.; Antonelli, M.; Wiesner, M. R., Influence of Aqueous Inorganic Anions on the Reactivity of Nanoparticles in TiO_2 Photocatalysis. *Langmuir* **2017,** *33*, (11), 2770-2779.

12. Chong, M. N.; Jin, B.; Chow, C. W. K.; Saint, C., Recent developments in photocatalytic water treatment technology: A review. *Water Res.* **2010,** *44*, (10), 2997-3027.

13. Linsebigler, A. L.; Lu, G.; Yates, J. T., Jr., Photocatalysis on TiO_2 Surfaces: Principles, Mechanisms, and Selected Results. *Chem. Rev.* **1995,** *95*, (3), 735-758.

14. Schneider, J.; Matsuoka, M.; Takeuchi, M.; Zhang, J.; Horiuchi, Y.; Anpo, M.; Bahnemann, D. W., Understanding TiO_2 Photocatalysis: Mechanisms and Materials. *Chem. Rev.* **2014,** *114*, (19), 9919-9986.

15. Chen, D.; Cheng, Y.; Zhou, N.; Chen, P.; Wang, Y.; Li, K.; Huo, S.; Cheng, P.; Peng, P.; Zhang, R.; Wang, L.; Liu, H.; Liu, Y.; Ruan, R., Photocatalytic degradation of organic pollutants using TiO_2-based photocatalysts: A review. *J. Cleaner Prod.* **2020,** *268*, 121725.

16. Friedmann, D.; Mendive, C.; Bahnemann, D., TiO_2 for water treatment: Parameters affecting the kinetics and mechanisms of photocatalysis. *Appl. Catal., B* **2010,** *99*, (3), 398-406.

17. Ren, M.; Drosos, M.; Frimmel, F. H., Inhibitory effect of NOM in photocatalysis process: Explanation and resolution. *Chem. Eng. J.* **2018,** *334*, 968-975.

18. Brame, J.; Long, M.; Li, Q.; Alvarez, P., Inhibitory effect of natural organic matter or other background constituents on photocatalytic advanced oxidation processes: Mechanistic model development and validation. *Water Res.* **2015,** *84*, 362-371.

19. Awfa, D.; Ateia, M.; Fujii, M.; Yoshimura, C., Photocatalytic degradation of organic micropollutants: Inhibition mechanisms by different fractions of natural organic matter. *Water Res.* **2020,** *174*, 115643.

20. Wu, H.; Huang, L.; Rose, A.; Grassian, V. H., Impact of surface adsorbed biologically and environmentally relevant coatings on TiO_2 nanoparticle reactivity. *Environ. Sci.: Nano* **2020,** *7*, (12), 3783-3793.

21. Bui, H. T.; Park, H. Y.; Alvarez, P. J. J.; Lee, J.; Kim, W.; Kim, E.-J., Visible-Light Activation of a Dissolved Organic Matter–TiO_2 Complex Mediated via Ligand-to-Metal Charge Transfer. *Environ. Sci. Technol.* **2022,** *56*, (15), 10829-10837.

703 22. Long, M.; Brame, J.; Qin, F.; Bao, J.; Li, Q.; Alvarez, P. J. J., Phosphate Changes Effect
704 of Humic Acids on TiO_2 Photocatalysis: From Inhibition to Mitigation of Electron–Hole
705 Recombination. *Environ. Sci. Technol.* **2017,** *51*, (1), 514-521.
706 23. Mathew, R. A.; Wu, G.; Zhang, Y.; Shakiba, S.; Yao, Y.; Tsai, A.-L.; Louie, S. M.,
707 Natural organic matter adsorption conditions influence photocatalytic reaction pathways of
708 phosphate-treated titanium dioxide nanoparticles. *Environ. Sci.: Nano* **2021,** *8*, (8), 2165-2176.
709 24. Yuan, S.; Huang, J.; Qian, W.; Zhu, X.; Wang, S.; Jiang, X., Are Physical Sunscreens
710 Safe for Marine Life? A Study on a Coral–Zooxanthellae Symbiotic System. *Environ. Sci.*
711 *Technol.* **2023,** *57*, (42), 15846-15857.
712 25. Yang, S. P.; Bar-Ilan, O.; Peterson, R. E.; Heideman, W.; Hamers, R. J.; Pedersen, J. A.,
713 Influence of Humic Acid on Titanium Dioxide Nanoparticle Toxicity to Developing Zebrafish.
714 *Environ. Sci. Technol.* **2013,** *47*, (9), 4718-4725.
715 26. Keller, A. A., Nanomaterials in sunscreens: Potential human and ecological health
716 implications. *Int. J. Cosmet. Sci.* **2023,** *45*, (S1), 127-140.
717 27. Miller, R. J.; Bennett, S.; Keller, A. A.; Pease, S.; Lenihan, H. S., TiO2 Nanoparticles
718 Are Phototoxic to Marine Phytoplankton. *PLOS ONE* **2012,** *7*, (1), e30321.
719 28. Loddo, V.; Roda, G. C.; Parrino, F., Chapter 7. Kinetic Aspects of Heterogeneous
720 Catalytic Versus Photocatalytic Reactions. In *Heterogeneous Photocatalysis*, Marcì, G.;
721 Palmisano, L., Eds. Elsevier: 2019; pp 215-233.
722 29. Ohtani, B., Chapter 10 - Photocatalysis by inorganic solid materials: Revisiting its
723 definition, concepts, and experimental procedures. In *Advances in Inorganic Chemistry*, Eldik,
724 R. v.; Stochel, G., Eds. Academic Press: 2011; Vol. 63, pp 395-430.

30. Sauer, T.; Cesconeto Neto, G.; José, H. J.; Moreira, R. F. P. M., Kinetics of photocatalytic degradation of reactive dyes in a TiO_2 slurry reactor. *J. Photochem. Photobiol., A* **2002,** *149*, (1), 147-154.

31. Turolla, A.; Piazzoli, A.; Farner Budarz, J.; Wiesner, M. R.; Antonelli, M., Experimental measurement and modelling of reactive species generation in TiO_2 nanoparticle photocatalysis. *Chem. Eng. J.* **2015,** *271*, 260-268.

32. Wang, D.; Mueses, M. A.; Márquez, J. A. C.; Machuca-Martínez, F.; Grčić, I.; Peralta Muniz Moreira, R.; Li Puma, G., Engineering and modeling perspectives on photocatalytic reactors for water treatment. *Water Res.* **2021,** *202*, 117421.

33. Ollis, D. F., Kinetics of Liquid Phase Photocatalyzed Reactions: An Illuminating Approach. *J. Phys. Chem. B* **2005,** *109*, (6), 2439-2444.

34. Emeline, A. V.; Ryabchuk, V. K.; Serpone, N., Dogmas and Misconceptions in Heterogeneous Photocatalysis. Some Enlightened Reflections. *J. Phys. Chem. B* **2005,** *109*, (39), 18515-18521.

35. Pignatello, J. J.; Xing, B., Mechanisms of Slow Sorption of Organic Chemicals to Natural Particles. *Environ. Sci. Technol.* **1996,** *30*, (1), 1-11.

36. Shakiba, S.; Hakimian, A.; Barco, L. R.; Louie, S. M., Dynamic Intermolecular Interactions Control Adsorption from Mixtures of Natural Organic Matter and Protein onto Titanium Dioxide Nanoparticles. *Environ. Sci. Technol.* **2018,** *52*, (24), 14158-14168.

37. Aljeddani, G. S.; Alghanmi, R. M.; Hamouda, R. A., Study on the Isotherms, Kinetics, and Thermodynamics of Adsorption of Crystal Violet Dye Using Ag-NPs-Loaded Cellulose Derived from Peanut-Husk Agro-Waste. In *Polymers*, 2023; Vol. 15.

38. Schwarzenbach, R. P.; Gschwend, P. M.; Imboden, D. M., Chapter 15. Direct Photolysis. In *Environmental Organic Chemistry*, Second ed.; Wiley: 2002; pp 611-654.

39. Wu, H.; Gonzalez-Pech, N. I.; Grassian, V. H., Displacement reactions between environmentally and biologically relevant ligands on TiO_2 nanoparticles: insights into the aging of nanoparticles in the environment. *Environ. Sci.: Nano* **2019,** *6*, (2), 489-504.

40. Kim, J.; Doudrick, K., Emerging investigator series: protein adsorption and transformation on catalytic and food-grade TiO_2 nanoparticles in the presence of dissolved organic carbon. *Environ. Sci.: Nano* **2019,** *6*, (6), 1688-1703.

41. Balasubramanian, G.; Dionysiou, D. D.; Suidan, M. T.; Subramanian, V.; Baudin, I.; Laîné, J. M., Titania powder modified sol-gel process for photocatalytic applications. *J. Mater. Sci.* **2003,** *38*, (4), 823-831.

42. Carbonaro, S.; Sugihara, M. N.; Strathmann, T. J., Continuous-flow photocatalytic treatment of pharmaceutical micropollutants: Activity, inhibition, and deactivation of TiO_2 photocatalysts in wastewater effluent. *Appl. Catal., B* **2013,** *129*, 1-12.

43. Gao, F.; Wang, J.; Zhang, H.; Hang, M. A.; Cui, Z.; Yang, G., Interaction energy and competitive adsorption evaluation of different NOM fractions on aged membrane surfaces. *J. Membr. Sci.* **2017,** *542*, 195-207.

44. Mowla, M.; Shakiba, S.; Louie, S. M., Selective quantification of nanoplastics in environmental matrices by asymmetric flow field-flow fractionation with total organic carbon detection. *Chem. Commun.* **2021,** *57*, (96), 12940-12943.

45. National Institute of Standards and Technology (NIST). *Certificate of Analysis: SRM 1898 - Titanium dioxide nanomaterials*; Gaithersburg, MD, 2020.

46. Bates, D. M.; Watts, D. G., *Nonlinear regression analysis and its applications*. Jon Wiley & Sons: New York, NY, 1988.

47. Yuan, Y.; Mortazavi, M.; Garg, S.; Ma, J.; Waite, T. D., Comparison of Performance of Conventional Ozonation and Heterogeneous Catalytic Ozonation Processes in Phosphate- and Bicarbonate-Buffered Solutions. *ACS EST Engg.* **2022,** *2*, (2), 210-221.

48. Darmograi, G.; Prelot, B.; Geneste, A.; De Menorval, L.-C.; Zajac, J., Removal of three anionic orange-type dyes and Cr(VI) oxyanion from aqueous solutions onto strongly basic anion-exchange resin. The effect of single-component and competitive adsorption. *Colloids Surf., A* **2016,** *508*, 240-250.

49. Conkle, J. L.; Lattao, C.; White, J. R.; Cook, R. L., Competitive sorption and desorption behavior for three fluoroquinolone antibiotics in a wastewater treatment wetland soil. *Chemosphere* **2010,** *80*, (11), 1353-1359.

783 **For Table of Contents Only**

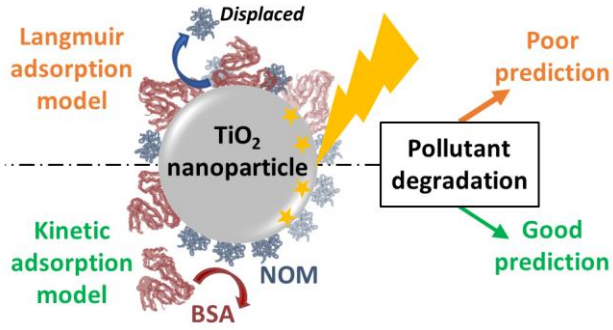

784